



## Accumulation of nanocarriers in the ovary: A neglected toxicity risk?

Andreas Schädlich<sup>a</sup>, Stefan Hoffmann<sup>a</sup>, Thomas Mueller<sup>b</sup>, Henrike Caysa<sup>a,b</sup>, Cornelia Rose<sup>c</sup>, Achim Göpferich<sup>c</sup>, Jun Li<sup>a</sup>, Judith Kuntsche<sup>a</sup>, Karsten Mäder<sup>a,\*</sup>

<sup>a</sup> Martin Luther University Halle-Wittenberg, Department of Pharmaceutical Technology and Biopharmaceutics, D-06120 Halle (Saale), Germany

<sup>b</sup> Martin Luther University Halle-Wittenberg, Department of Internal Medicine IV, Oncology/Hematology, D-06120, Halle (Saale), Germany

<sup>c</sup> University of Regensburg, Department of Pharmaceutical Technology, D-93053, Regensburg, Germany

### ARTICLE INFO

#### Article history:

Received 3 October 2011

Accepted 10 February 2012

Available online 21 February 2012

#### Keywords:

Nanocarrier

Nanoparticle

Toxicity

*In vivo* imaging

Fluorescence imaging

Ovary

### ABSTRACT

Several nanocarrier systems are frequently used in modern pharmaceutical therapies. Within this study a potential toxicity risk of all nanoscaled drug delivery systems was found. An accumulation of several structurally different nanocarriers but not of soluble polymers was detected in rodent ovaries after intravenous (*i.v.*) administration. Studies in different mouse species and Wistar rats were conducted and a high local accumulation of nanoparticles, nanocapsules and nanoemulsions in specific locations of the ovaries was found in all animals. We characterised the enrichment by *in vivo* and *ex vivo* multispectral fluorescence imaging and confocal laser scanning microscopy. The findings of this study emphasise the role of early and comprehensive *in vivo* studies in pharmaceutical research. Nanocarrier accumulation in the ovaries may also comprise an important toxicity issue in humans but the results might as well open a new field of targeted ovarian therapies.

© 2012 Elsevier B.V. All rights reserved.

### 1. Introduction

Today various types of nanocarrier formulations like liposomes, nanoparticles, nanocapsules, nanotubes and others are intensively investigated or already commercially available [1–3]. Those nanoscaled drug delivery systems are commonly used in clinical therapy and in research to enhance circulation time or to achieve passive drug targeting [4–6]. Although toxicity and potential risks of such carriers have already been studied in detail, many effects are still poorly understood [7]. Unexpected accumulation of drug delivery systems in specific regions after intravenous (*i.v.*) injection could result in harmful side effects. Therefore, potential accumulation of nanocarriers in various tissues should be investigated during the development of new drug carrier systems. The fate of the carriers in the body depends mainly on their size, charge, shape and flexibility. Carriers larger than 150 nm often accumulate in liver and spleen, whereas very small carriers like polymers with hydrodynamic diameters <8 nm, can be rapidly eliminated by the kidneys [2,3,8–11]. Studies have also shown that liposomes <70 nm are eliminated faster than larger ones due to extravasation and accumulation in the parenchymal cells of the liver [12,13]. Therefore, *in vivo* distribution, accumulation and elimination studies must be combined with particle size analysis to obtain a comprehensive understanding of the properties of modern drug formulations.

Until now, a possible accumulation in ovarian tissue has not been investigated in biodistribution studies of nanocarriers. Therefore, extensive *in vivo* and *ex vivo* studies were performed within this study to examine this in detail. In our present study we measured the accumulation of differently composed nanoscaled drug delivery systems in the ovaries of rodents. To investigate the correlation of carrier size and ovary accumulation, detailed size distributions of all systems were measured by asymmetrical flow-field-flow fractionation (AF4). The accumulation in ovaries was characterized *in vivo* and *ex vivo* in different mouse strains and Wistar rats using non-invasive fluorescence imaging and confocal laser scanning microscopy (CLSM). Fluorescence imaging is a powerful technique to investigate the body fate of drug delivery systems noninvasively over several hours up to days or months in the same organism. The fluorescence imaging studies were carried out using consequently near infrared (NIR) fluorescent dyes that provided information also from deep tissues as well as from tissues which are highly supplied with blood. Those dyes were either covalently stable bound via amide bonds (polymers) or physically entrapped into the carriers (nanoparticles, nanocapsules and nanoscaled lipid emulsion). In total, we were able to prove the ovary accumulation of 5 different nanocarrier batches with diameters between 45 and 350 nm.

### 2. Materials and methods

#### 2.1. Materials

3,6-dimethyl-1,4-dioxan (D,L-lactide), poly(ethylene glycol) monomethyl ether (mPEG2000; MW = 2000 Da), stannous 2-ethylhexanoate

\* Corresponding author. Tel.: +49 345 5525167; fax: +49 345 5527029.

E-mail address: [karsten.maeder@pharmazie.uni-halle.de](mailto:karsten.maeder@pharmazie.uni-halle.de) (K. Mäder).

(>95%), 1,1'-Dioctadecyl-3,3',3'-tetramethylindocarbocyanine perchlorate (DiI), 3,3'-Dioctadecyloxycarbocyanine perchlorate (DiO), ethylene diamine, toluene sulfonyl chloride and sorbitol were obtained from Sigma Aldrich, Germany. Sucrose was obtained from Merck KGaA, Germany and poloxamer 188 (Pluronic F68) from Riedel-de Haën, Germany. The fluorescence dye 1,1'-dioctadecyl-3,3',3'-tetramethylindocarbocyanine iodide (DiR) was purchased from Invitrogen, Germany. The fluorescence dye IRDye 800CW was obtained from LI-COR, US. The diblock copolymer PLGA-PEG 45–5 (PLGA 50:50 45 kDa and PEG 5 kDa) and the Lipofundin 20 N were purchased from Boehringer Ingelheim, Germany and Lipiodol (Lipiodol Ultra fluid) from Guerbet GmbH, Germany. Hydroxyethyl starch 200/0,5 (batch HES) and dextran 500 (batch DEX) were kindly provided by Serumwerke Bernburg AG, Germany. Formaldehyde was purchased from Carl Roth GmbH, Germany. All other substances and solvents were used as received.

## 2.2. Preparation of nanoparticles

As described earlier [14] a nanoprecipitation method was used for the preparation of 3 NIR fluorescent nanoparticle batches, differing in size (batch NP1–NP3, Table 1). 37.5 mg (batch NP1) PEG<sub>2</sub>PLA<sub>20</sub> or PEG<sub>2</sub>PLA<sub>40</sub> (50 mg for batch NP2 or 100 mg for batch NP3), the numbers refer to the molecular weight in kDa, were dissolved in 5 mL chloroform. Referring to the polymer, 0.5% (batch NP1) or 1.0% (batch NP2 and NP3), of the NIR emitting fluorescence dye 1,1'-dioctadecyl-3,3',3'-tetramethylindocarbocyanine iodide (DiR) were added. To form solid nanoparticles, the solution was dropped into 40 mL of an aqueous solution containing 0.25% Pluronic F68. After removal of organic solvent by evaporation, the nanoparticles were collected by centrifugation and washed with purified water. Subsequently 5% sucrose was added and the dispersion was freeze-dried.

## 2.3. Preparation of nanocapsules

Nanocapsules were prepared by interfacial polymer deposition after solvent displacement (batch NC, Table 1). 20 mg PLGA-PEG

45–5 (PLGA (45 kDa) and PEG (5 kDa), 50:50) and 50 µL Lipiodol, loaded with 100 µg DiR (batch NC) or with 100 µg DiI (batch NC-DiI, Table 1) were dissolved in 2 mL acetone. The solution was dropwise injected into 4 mL water under stirring. The acetone was evaporated (under reduced pressure at 30 °C) and all samples were centrifuged (for 15 min at 4000 rpm) using a MiniSpin from Eppendorf, Germany. The supernatant containing dye loaded nanocapsules was 2 mL.


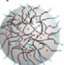
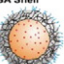
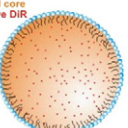
## 2.4. Dye loading of a nanosized lipid emulsion

For comparison also a commercially available lipid emulsion (Lipofundin 20 N) was loaded with DiR. An ethanolic DiR solution (100 µg/ mL) was dropwise added under continuous stirring (batch LE, Table 1) to get a final dye loading with the same fluorescence intensity as it was achieved for the nanocapsule batch.

## 2.5. Preparation of soluble polymers

Hydroxyethyl starch (batch HES, Table 1) and dextran (batch DEX, Table 1) were amino-modified using ethylene diamine and covalently coupled with the NIR-fluorescent dye IR800CW. The amino groups were introduced to the molecules based on a previously described method [16]. Toluene sulfonyl chloride (0.5 g) was slowly added to a DMF solution (30 mL) of 1 g polymer and 1 mL triethyl amine. The mixture was cooled on ice and reacted for 2 h in the dark. After precipitating in acetone, the polymers were dialysed against water (3.5 kDa membrane from Spectrum Labs, United States) and subsequently freeze dried. The tosyl-modified polymers (0.25 g) were reacted with ethylene diamine (1.5 g) in DMF (50 mL) and borax buffer (pH 10) for 20 h. Resulting polymers were precipitated in methanol and isopropanol (1:1), afterwards several times dialysed against water and subsequently lyophilised. The amino-modified polymers (100 mg) were dissolved in water (50 mL), reacted with 0.5 mg IRDye 800CW in the dark for 3 h and once again dialysed against water and afterwards lyophilised.

**Table 1**  
Composition and particle sizes of used nanocarriers.

	Batch	Polymer/ carrier	Size	Animals per batch
<b>Polymers (flexible)</b>				
HES/ dextran polymer dye IR800 	Batch HES	HES 200	30 nm (D <sub>w</sub> ) <sup>a)</sup>	3 SKH1 mice (♀)
	Batch DEX	Dextran 500	35 nm (D <sub>w</sub> ) <sup>a)</sup>	
<b>Nanoparticles (solid)</b>				
PEG-PLA particle dye DiR 	Batch NP1	PLA <sub>20</sub> PEG <sub>2</sub>	45 nm (D <sub>50</sub> ) <sup>b)c)</sup>	4 SKH1 mice (♀)
	Batch NP2	PLA <sub>40</sub> PEG <sub>2</sub>	65 nm (D <sub>50</sub> ) <sup>b)c)</sup>	3 SKH1 mice (♂)
	batch NP3	PLA <sub>40</sub> PEG <sub>2</sub>	100 nm (D <sub>50</sub> ) <sup>b)c)</sup>	
<b>Nanocapsules (solid shell)</b>				
PEG-PLGA Shell dye DiR oil core 	Batch NC	PLGA <sub>45</sub> PEG <sub>5</sub> , Lipiodol	55 nm (D <sub>50</sub> ) <sup>b)</sup>	4 SKH1 mice (♀) <sup>d)</sup>
	Batch NC-DiI <sup>d)</sup>	PLGA <sub>45</sub> PEG <sub>5</sub> , Lipiodol	Not determined	3 BALB/c mice (♀) <sup>d)</sup> 3 Wistar rats (♀) <sup>d)</sup>
<b>Nanosized lipid emulsion droplets</b>				
lecithine oil core dye DiR 	Batch LE	Lipofundin 20 N	350 nm (D <sub>50</sub> ) <sup>b)</sup>	4 SKH1 mice (♀)

<sup>a)</sup> D<sub>w</sub> means the weight-average mean square diameter, measured by AF4/MALLS.

<sup>b)</sup> D<sub>50</sub> means the mass weighted distribution median diameter, measured by AF4/MALLS.

<sup>c)</sup> D<sub>50</sub> values were published previously [15].

<sup>d)</sup> Batch NC-DiI was only used for additional confocal microscopy studies. It was injected into 2 SKH1-Hr<sup>hr</sup> mice (♀).

## 2.6. Particle size measurement

All nanocarrier batches were analysed by AF4 based on a method previously described [14]. The fractionation system (AF4/ MALLS) was composed of an Eclipse AF4 (Wyatt, Germany) which was coupled with a multi-angle laser light scattering (MALLS) detector (DAWN EOS, Wyatt). Particles were separated in a trapezoidal-shaped channel (length 265 mm, largest width 21 mm, height 350  $\mu\text{m}$ ) in dependence on their size and shape by applying appropriate cross flow rates. A 5 kDa membrane (regenerated cellulose or polyethersulfone (MWCO 5 kDa, Microdyn-Nadir, Germany) was used as accumulation wall. Bi-distilled water served as carrier liquid (preserved with 0.02% sodium azide and filtered through 0.1  $\mu\text{m}$  pore sized filter). A volume of 100  $\mu\text{L}$  of the nanocarrier dispersions (1 mg/mL for batch NP1–NP3, for batch NC and for batch HES and batch DEX, 0.1 mg/mL for batch LE) was injected during focusing (focus flow 2 mL/min). Samples were eluted with a constant (1 mL/min) and decreasing cross-flow (from 2 to 0.5 mL/min within 5 min and from 0.5 to 0 mL/min within 35 min). The particle sizes were calculated based on the light scattering signal. For the batches NP1–NP3, NC and LE the particle mode was used for size evaluations (assuming compact spheres), whereas for the polymers the molecular weight mode was used. The Astra software 4.90 (Wyatt, Germany) allowed determining the corresponding mean diameters (D50) from the mass weighted distributions [14]. Polymer sizes were calculated based on weight-average mean square diameters ( $D_w$ ) using RI detector signal. All dispersions were measured in triplicate, and results are given as average in Table 1.

## 2.7. Animal handling

All experiments complied with the standards for use of animal subjects as stated in the guideline from the animal care- and use-committee of Saxony Anhalt. As listed in Table 1 *in vivo* studies were performed in pubescent female (batches NP1–NP3, NC and LE, all in quadruplicate, batches HEX and DEX in triplicate and batch NC–DiI in duplicate) and male (batches NP1–NP3, all in triplicate), nude SKH1–*Hr<sup>hr</sup>* mice (age: 2–12 months). Further *in vivo* studies were performed in female BALB/c mice (batch NC, n = 3, age: 6 months) and in female Wistar rats (batch NC, n = 3, age: 12 months). The animals were housed under controlled conditions (12 h light/dark schedule, 24 °C). Respective samples were isotomised with sorbitol and slowly *i.v.* injected into the tail vein (100  $\mu\text{L}$  for mice and 1 mL for rats, in a concentration of 8 mg/mL for the nanoparticle and nanocapsule batches and 10 mg/mL for the polymers). For *in vivo* fluorescence imaging, the mice were anaesthetised using a mixture of isoflurane and oxygen with an initial flow of 4% isoflurane (3.0 L/min oxygen) and a steady state flow of 1.8% isoflurane (1.5 L/min oxygen). The mice were placed on a 35 °C temperature-controlled heating plate to prevent a decrease of body temperature. For *ex vivo* analysis mice and rats were sacrificed using carbon dioxide 24 h after injection.

## 2.8. Fluorescence imaging

*In vivo* and *ex vivo* fluorescence imaging experiments were performed using the Maestro *in vivo* fluorescence imaging system (CRI, now Caliper Life Sciences, United States) and the Maestro software (version 2.10) [14,15]. The NIR filter set (710–760 nm excitation and 800 nm long-pass emission filter) was used for the detection of both NIR dyes, the DiR and the IRDye 800CW. The measurement files (cubes) were grabbed in the spectral range between 780 and 950 nm using auto exposure times. The tuneable filter was automatically stepped in 10 nm increments and intensity weighted greyscale images were acquired at each step.

The single spectral species were unmixed from the recorded cubes using reference spectra of DiR or IRDye 800CW and the background signal of an untreated mouse that was measured under same conditions.

During the unmixing process, each pixel was intensity weighted allocated to the respective reference spectra. The resulted greyscale images of the respective fluorescence signals were used for further analysis or to generate jet color images [14]. Those have an intensity weighted incremental color profile. Pixels with maximum intensities are set to dark red and pixels with no fluorescence to dark blue/black. In between there is a graduation from red to orange, yellow, light and dark blue.

For *ex vivo* analysis, the mice and rats were sacrificed 24 h after injection. The uteri with ovaries (female mice and rats) or seminal vesicles, testes (male mice) were excised and imaged with highest possible magnification on a plastic plate. The spectral species were unmixed from the image cubes as described above. Ovaries and uteri from untreated mice served as negative controls.

For batches NP1–NP3, the accumulation in the ovaries was also compared with the distribution of the nanoparticles in other organs and tissues. Therefore, the intestine, fat, liver, gall bladder, lung, spleen, kidney and heart were placed next to uterus with ovaries into 9 separate holes of a 24 holes well-plate. This allowed reproducible measurement conditions for the organs and tissues of all mice. The plate was imaged with the Maestro *in vivo* imaging system. To detect also minor nanocarrier accumulations, the measurements were repeated after masking the liver with a black plastic plate. Organs from untreated mice served as negative controls. A region of interest (ROI) in the size of the well-plate hole (1.9  $\text{cm}^2$ ) was generated to extract total and maximum intensities of the organs and tissues. The software correlated them to the respective exposure times. To exclude intensity variations due to different initial dye concentrations and intensities between the 3 different nanoparticle batches (NP1–NP3), a previously described correction method was applied [14]: For this, the total signal (correlated to the exposure time) was divided by the *in vitro* emission peak maximum which was determined prior to the *in vivo* measurements. All values were normalised to 100% referring to the highest result.

## 2.9. Confocal laser scanning microscopy (CLSM)

CLSM experiments were carried out using a LSM 710 (Zeiss, Germany). Dyes were excited using an Ar-Laser for DiI (514 nm) and DiO (488 nm) and a HeNe-Laser for DiR (633 nm). Samples were prepared from just extracted ovaries that were cut into small slices of app. 0.5 mm using a razor blade. Afterwards the slices were transferred to an object slide. Further, frozen sections of extracted ovaries were stained with DiO to visualise the cellular membranes. The 40x or the 63x Plan Apo oil immersion objectives were used for microscopy. For comparison, also a pure solution of DiI stained nanocapsules was imaged under the same conditions like the sliced ovaries. To obtain a 3-dimensional impression of the nanoparticles distribution in the microscopic ovary structures Z-stacks were applied using 80  $\mu\text{m}$  steps. All images were grabbed and processed with scale bars using the software ZEN 2008 (version 1.0.3).

## 2.10. Light microscopy

An Axiolab Microscope from Carl Zeiss MicroImaging (Germany) was used for light microscopy of ovarian tissue. Excised ovaries were fixed with 4% paraformaldehyde and embedded in paraffin. Thin slices (4  $\mu\text{m}$ ) were cut using a microtome and transferred to object slides. The slices were dewaxed and stained with Haematoxylin and Eosin. Images were grabbed and processed using the Zeiss Axio-lab software.

## 3. Results

### 3.1. Particle size measurements

For particle size measurements AF4 was combined with MALLS. This allowed accurate size evaluation of all batches due to sample

separation prior size determination. The characteristic D50 (for nanocarriers) and  $D_w$  (for polymers) are shown in Table 1. All used nanocarriers were within the size range between 45 and 350 nm, whereas diameters of 30 and 35 nm were measured for the flexible polymers with the covalently bound NIR dye. The lipid nanoemulsion was rather broad distributed. All nanoparticle batches were narrow distributed [15]. Based on the determined D50 values of 45 nm (batch NP1), 65 nm (batch NP2) and 100 nm (batch NP3) it is possible to draw conclusions about the size dependent accumulation of nanocarriers in rodent ovaries.

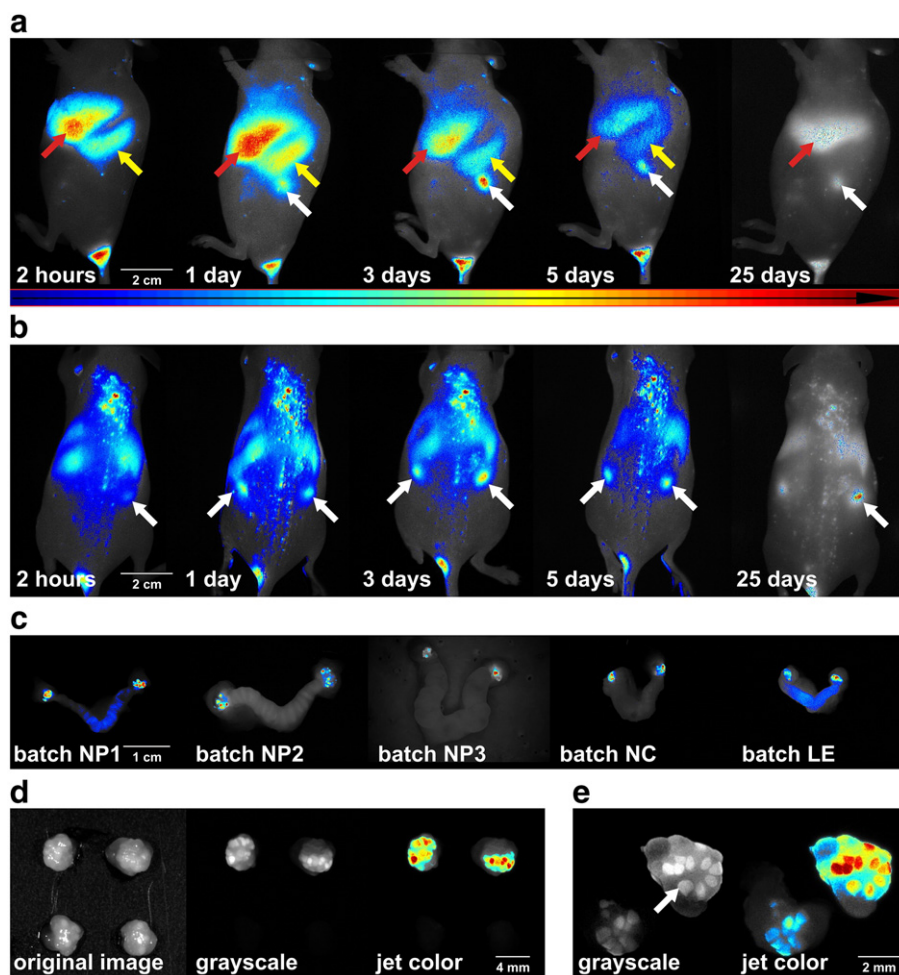
### 3.2. *In vivo* and *ex vivo* fluorescence imaging studies

Within this study, the ovary accumulation of 7 differently composed nanoscaled drug delivery systems (Table 1) was investigated using the Maestro *in vivo* imaging system. For our study we selected NIR fluorescent dyes, as they can be detected also in deep tissues [17]. Generally, fluorescent dyes can be loaded to the carrier systems by incorporation or by covalent attachment. As incorporation of the fluorescent dye does normally not affect the surface characteristics of the nanocarriers, this method was used for the nanoparticle, nanocapsule and lipid nanoemulsion batches. In case of soluble polymers (batches HES and DEX) the fluorescent dye was covalently

coupled to the polymer. For a physical entrapment, a very hydrophobic dye is required which will not diffuse out of the drug delivery system until the carrier is degraded. Therefore, dialkylcarbocyanine dyes (DiR and DiI) were chosen. DiR is a very lipophilic NIR fluorescence dye that has already been used in several *in vivo* studies to track nanocarriers by fluorescence imaging noninvasively [18,19]. A distinct diffusion of the dye out of the nanocarriers into the blood can be excluded due to the very high partition coefficient of the utilised dye. Reported log P values of dialkylcarbocyanine dyes are between 17 [20] and 20 [21]. The release of those dyes from lipophilic nanocarriers is reported to be less than 4% within the first week [22,23].

In this study (Table 1) DiR was incorporated into 3 batches of different sized PEG-PLA nanoparticles (batch NP1: PEG<sub>2</sub>PLA<sub>20</sub>, batch NP2 and NP3: PEG<sub>2</sub>PLA<sub>40</sub>), 1 batch of oil loaded PEG<sub>5</sub>PLGA<sub>45</sub> nanocapsules (batch NC) and 1 batch of a common lipid emulsion (Lipofundin 20 N, batch LE). Due to the fact that a physical incorporation is not possible for soluble hydrophilic polymers, the 2 polymer batches HES and DEX were successfully amino-modified and covalently stable labelled with the amine reactive NIR fluorescent dye IR 800CW (NHS-ester).

The long-term *in vivo* fate was investigated over about 3 weeks in nude female mice (SKH1-Hr<sup>hr</sup>). Detailed *in vivo* distribution studies as



**Fig. 1.** *In vivo* and *ex vivo* fluorescence images of accumulated nanocarriers. a, Time dependent lateral optical images of a nude mouse after *i.v.* nanoparticle injection (batch NP2) presented as an intensity weighted visualization of the extracted fluorescence dye signal (jet color). Areas with highest dye intensities are red and those with lowest dye concentrations are blue. The red arrow marks the liver, the yellow one the spleen and the white one the ovaries. b, Intensity weighted jet color images of the dorsal side from the same mouse as shown in a (arrows point to ovaries). The long term enrichment of the carrier system in the ovaries is visible. c, *Ex vivo* jet color images of the excised uterus with ovaries 24 h after nanocarrier injection. While the uterus is not or only slightly fluorescent, high fluorescence intensities were detected in the ovaries. d, *Ex vivo* images of excised ovaries (original photograph (from left to right), grayscale image of the extracted dye signal and corresponding jet color image for a better visualization of the intensity allocation), 24 h after batch NP3 administration (upper row), negative control (lower row). e, Grayscale and corresponding jet color image of the sliced ovary in the highest possible magnification. The fluorescence in the ovaries is concentrated in highly fluorescent spots (marked by arrow).

well as size dependent tumor accumulation studies of used nanoparticle batches NP1–NP3 have been discussed previously [14,15]. The resulting *in vivo* images are exemplarily shown for medium sized batch NP2 (PEG<sub>2</sub>PLA<sub>40</sub>) nanoparticles in Fig. 1a and b.

An accumulation of the nanoparticles in the organs of the RES was already observed after 2 h. One day after injection, the fluorescence intensity in the RES reached maximum values and decreased continuously thereafter. Additionally, an accumulation of the nanoparticles in the ovaries (Fig. 1a and b marked by white arrows) was detectable already 2 h after administration. The fluorescence intensity from the ovaries further increased within 24 h and remained constant at a high level over several days. Even 25 days after injection a bright fluorescence signal could be detected noninvasively in the area of the ovaries *in vivo*.

To confirm the ovarian accumulation of nanoparticles, *ex vivo* experiments with all 3 nanoparticle batches were conducted. For that purpose the uteri with ovaries were excised 24 h after *i.v.* injection. Representative *ex vivo* images are presented in Fig. 1c. As it is visible exemplarily in the first 3 images, strong fluorescence intensities were detected in the ovaries of all 12 mice that were treated with nanoparticles (batch NP1–batch NP3). To evaluate if this observation is not related to the type of nanocarrier e.g. due to a characteristic property of the polymer surface, the experiment was repeated with 2 further nanoscaled formulations (batch NC and batch LE) with a completely different composition. Representative images are shown in Fig. 1c. As it is clearly visible in all images, the uterus itself was low or even not fluorescent. However, the ovaries of all 20 mice were highly fluorescent independently of the size and the surface properties of the administered nanocarrier batches.

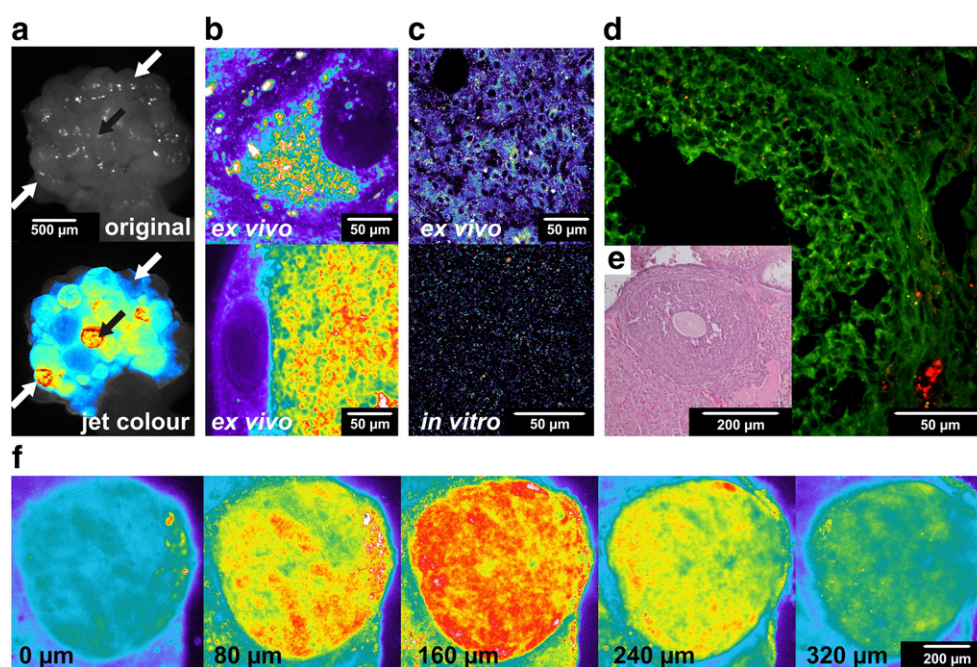
To exclude the possibility of measurement artefacts, the ovaries of treated (batch NP2) and untreated mice were measured simultaneously (Fig. 1d). The resulting images of the isolated DiR signal indicate a high nanocarrier accumulation in fluorescent spots whereas no fluorescence at all was found in the control tissues. Magnified images of sliced ovaries, shown in Fig. 1e, confirmed the local and punctual enrichment. To eliminate the possibility of a species specific accumulation in SKH1-Hr<sup>hr</sup> mice, *in vivo* and *ex vivo* studies with oil loaded PEG<sub>5</sub>PLGA<sub>45</sub>

nanocapsules were repeated in 3 female BALB/c mice and 3 Wistar rats. Comparable accumulation results were found in all of the experiments.

An original photograph of the excised rat ovary in comparison to the corresponding intensity weighted jet color image of the same part is shown in Fig. 2a. Due to the increased size of the rat ovary compared to the mouse ones more details are distinguishable. Also in the ovaries of the Wistar rats, local accumulations of the nanocapsules in varying intensities and tissue depths were detectable (marked by arrows in Fig. 2a). The direct comparison of both images also shows that some ball like structures visible in the original photograph are not fluorescent, whereas others are highly fluorescent. This fact indicates that the nanocarrier accumulations might depend on the progress stage within the ovarian cycles.

### 3.3. Confocal microscopy studies

To characterise the local areas of highest fluorescence intensities in more detail, confocal microscopy studies were conducted. Z-stack CLSM images (80  $\mu\text{m}$  steps) confirmed the accumulation in round, ball like tissue structures with an average diameter of approximately 200–300  $\mu\text{m}$  (Fig. 2f). No fluorescence signals were detected in the area of nuclei-like structures (Fig. 2b). However, by CLSM highly fluorescent spots in the ovarian tissue (Fig. 2c, top image) were assignable to the injected nanocarrier dispersion (lower image). In combination with the *in vivo* results presented in Fig. 1a and b, where fluorescence in the ovaries was detectable for more than 25 days a local long term release of incorporated dyes or drugs from the nanocarriers can be expected. *Ex vivo* studies were extended by frozen section sliding of excised tissues. In Fig. 2d, accumulated nanoparticles (red) are visible next to cells where the cellular membrane was stained with DiO (green). Fig. 2e shows a stained light microscopic picture of a growing follicle from mouse ovarian tissue.



**Fig. 2.** *Ex vivo* fluorescence images, confocal and light microscopic pictures of ovarian tissue. a, *Ex vivo* photograph (top) and corresponding jet color image (bottom) of a rat ovary (batch NC). Arrows point to same positions and mark characteristic ball like regions. b, Intensity weighted CLSM images of ovarian tissue (batch NP3). c, CLSM images (batch NC-DiI) of ovarian tissue from a treated mouse (top, *ex vivo*) in comparison to the *in vitro* NC-DiI dispersion (bottom). d, Frozen section CLSM image of excised ovary tissue, batch NP3 (red), cells stained with DiO (green). e, Light microscopic picture of ovarian tissue, stained with haematoxylin and eosin. f, Z-stack series of intensity weighted CLSM images (80  $\mu\text{m}$  steps) of ovarian tissue (batch NC-DiI).

### 3.4. Size dependent *ex vivo* fluorescence imaging analysis

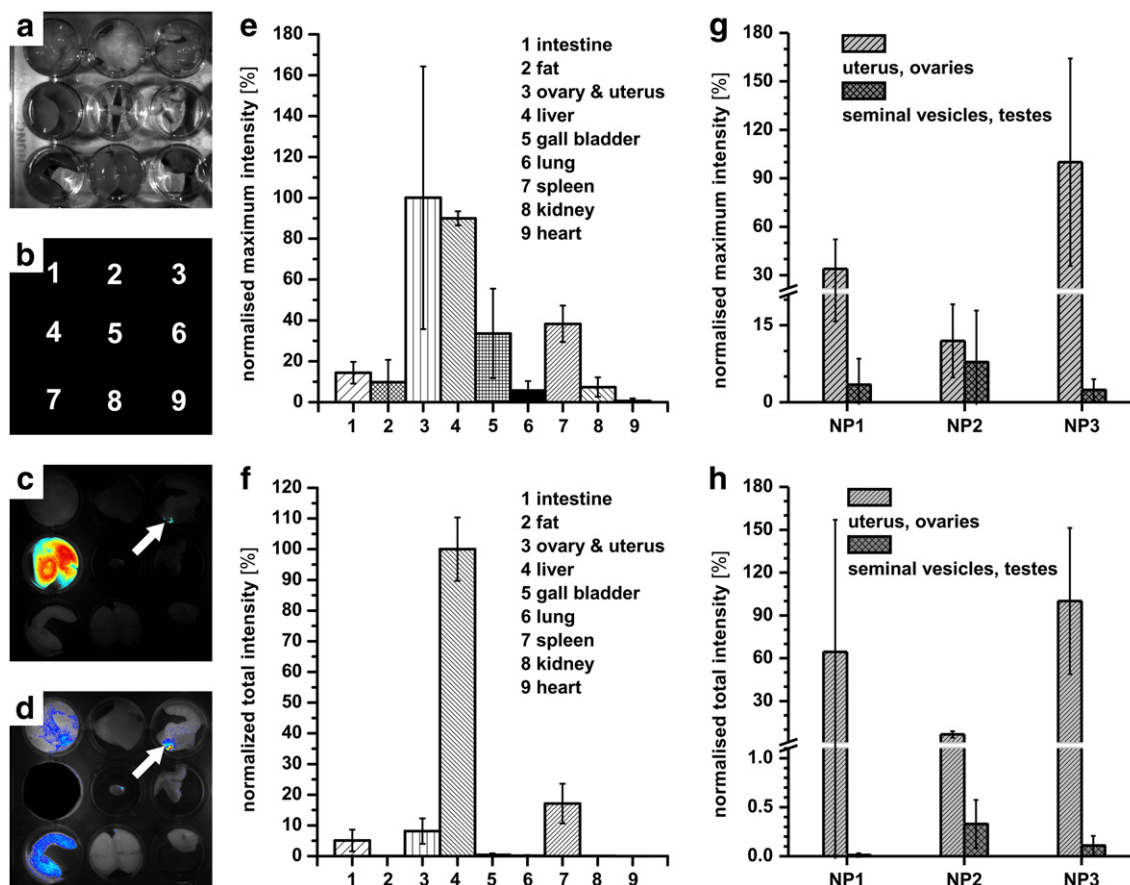
To investigate a potential size dependent accumulation of nanocarriers in the ovaries *ex vivo* studies of 3 nanoparticle batches (batch NP1–NP3), varying in particle sizes (Table 1) were performed. Nine organs of each mouse (known for nanocarrier accumulation or excretion) were placed, each into a separate hole of a 24 holes well-plate (Fig. 3a). All organs in the well-plate were imaged simultaneously. The well plate allowed the arranging of the tissues and organs of each mouse in the same position for all fluorescence imaging measurements and thus ensured reproducible measurement conditions. The intensity weighted DiR signal as a jet color images are shown in Fig. 3b–d. Organs from untreated mice were imaged as a control. Accumulations in the liver (dark red) as well as in small parts of the ovary (marked by arrow) are visible (Fig. 3c). After covering the liver with a black plastic plate, also weak fluorescence signals from intestine and spleen were detectable (Fig. 3d).

Based on the measured DiR intensity signals, normalised maximum and total intensities of all excised organs were calculated. Corresponding graphs are displayed exemplarily for batch NP3 in Fig. 3e and f. The maximum fluorescence intensity, measured from local spots of the ovaries, was as high as it was detected in the liver, which is the major organ for nanocarrier elimination within the RES. Related to that, the spleen and the gall bladder showed half maximum intensities. All other organs and tissues had intensities near the detection limit. The maximum intensity values allow a comparison of accumulations in organs differing in size. A high enrichment situated

only in a local part of a tissue for example leads to high maximum intensity values, but the total signal of the same sample, as the sum of all pixels, would only be slightly increased. Thus, the normalised total intensities yielded in divergent results compared to the normalised maximum intensities. The calculated total signal of the ovary with the uterus was below 10%, comparable to the much larger intestine. The difference between the total and the maximum signal (10 fold compared to liver results) underline the inhomogeneous and local nanoparticle accumulation in specific regions of the ovary as already above discussed for the *ex vivo* images.

As shown by the maximum intensities in Fig. 3g, nanoparticles from all 3 batches (NP1–NP3) accumulated in the ovaries. This corresponds to the analysis of the total intensities (Fig. 3h). Compared to male tissues (seminal vesicles and testes), the nanoparticle accumulation in the ovaries was reflected by a 20 fold higher maximum intensity and a 200 fold higher total intensity.

Normalised maximum intensities of batch NP1 and NP2 between 10 and 30% in comparison to 100% for batch NP3 indicate that bigger particles accumulated more than smaller ones, although the standard deviation is rather high here. A higher accumulation was also found by analyzing the total fluorescence intensities. Further investigations using small ( $\leq 35$  nm diameter) water soluble polymers (batch HES and batch DEX) were conducted to investigate whether there is a minimum size required for the accumulation of nanocarriers or not. For this purpose, a dose of 1 mg of each fluorescent labelled polymer in 100  $\mu$ L isotonic sorbitol solution was injected to the tail vein of 3 female mice (SKH1-Hr<sup>hr</sup>). No specific accumulation in mouse ovaries



**Fig. 3.** *Ex vivo* fluorescence images and analysis of different PEG-PLA nanoparticle batches (NP1–NP3). a–d, Original photograph (a) and jet color images of excised mouse organs from an untreated (b, negative control) and a treated (c and d) mouse (24 h after *i.v.* injection of batch NP3). For reproducible measurements, these were placed in the following order into 9 holes of a 24-well plate (related to b): intestine, fat, uterus with ovary, liver, gall bladder, lung, spleen, kidney and heart. Jet color images grabbed with 800 ms (c) and 1200 ms (d, liver was masked with a black plastic plate) exposure time. Both show the accumulation of nanoparticles in the RES and in the ovary (marked by white arrow). e and f, Normalised maximum (e) and total (f) fluorescence intensity graphs of organs, shown in c (n = 4). g and h, normalised maximum (g) and total (h) fluorescence intensity graphs of female and male genital tissues of the nanoparticle batches NP1–NP3 (female: n = 4, male: n = 3).

was found in any of the 6 treated mice. A minimum size limit above 35 nm diameter can be concluded from this experiment.

#### 4. Discussion

An accumulation of nanocarriers in the ovaries is mentioned in a small number of other publications based on *in vivo* and *ex vivo* studies with different kinds of nanoparticles and liposomes [24–30]. However, in all of them, the accumulation was neither investigated in detail nor thoroughly discussed. In these publications an ovary accumulation is (I) either visible in the presented pictures or (II) it can be derived from the presented data or (III) is briefly described. The reason, why the accumulation in rodent ovaries may not have attracted attention yet might be the fact that many research groups tend to use male mice. Another reason could be that the accumulation occurs only in mature, pubescent female mice. Furthermore, no accumulation in mouse ovaries was reported in a recent study of Daou *et al.* with very small nanoparticles (diameters below 50 nm) [31]. This might be related to the small size of the particles, which would correlate with our results, or to the mice age between 5 and 6 weeks, an age at which they were probably not yet pubescent. Another potential reason for the scarcity of published data on ovarian accumulation could be the observation that the nanocarrier accumulation appears to be restricted only to local parts of the ovaries. The overall amount of fluorescence signal from the ovaries was rather small (Fig. 3f) and not higher compared to other organs and tissues where no nanoparticles accumulated. Commonly, only the average amounts of the tissues or the percentages per administered dosages are compared in *in vivo* studies. Accumulations in the ovaries might thus often remain unnoticed. Few studies showed that an accumulation of nanoparticles in ovaries is detectable when the accumulation is calculated in  $\mu\text{g}$  per tissue weight (g) but not, when it is calculated as the percentage of the dose [26,30]. Anyhow, two fluorescence imaging studies of hybrid- and of lipid-nanoparticles also reported an accumulation [24,25]. Perez-Soler *et al.* even found liposome accumulations in the ovaries after subcutaneous injection [27]. Harrington *et al.* also detected a low but significant accumulation of pegylated, radiolabeled liposomes in the uterus and ovaries while non-pegylated liposomes were eliminated nearly completely within the first hour [28]. This short circulation time was probably not sufficient to achieve accumulations. Based on the size and structures of the accumulation areas from the *ex vivo* Maestro and CLSM images of our study, an enrichment in tertiary vesicular follicles might be possible but an accumulation in cells of the corpus luteum seem even more likely.

The corpus luteum is formed from the wall of the ruptured follicles after the ovulation. It is responsible for the production of progesterone which is a key factor during the pregnancy. Progesterone is in high concentrations needed shortly after the ovulation. Thus the ovarian corpus luteum grows and vascularizes extremely fast. Finally, the corpus luteum is typically very large in relation to the size of the ovary. It has been described that the rates of tissue growth and angiogenesis in the corpus luteum rival those of fast growing tumors [32]. This permits the assumption that an accumulation of nanocarriers in the corpus luteum is related to the EPR (enhanced permeability and retention) effect known for tumor tissues. Due to the EPR effect, *i.v.* injected nanocarriers can accumulate by passive diffusion due to a hyper-permeable tumor vasculature. By this, nanocarriers have the ability to be retained in tumor tissues which is a highly size dependent effect. An accumulation in the corpus luteum would be in agreement with the study of Thurston *et al.* They found accumulated liposomes in blood vessels around large ovarian follicles and in just formed corpora lutea but not inside follicles and only to a low degree in smaller, regressing corpora lutea [29].

Although the detailed mechanism still has to be enlightened, we could clearly prove specific nanocarrier accumulation in rodent ovaries. This effect might bear a potential toxicity risk if incorporated drugs are

locally released in the ovaries. Although, the overall amount was rather small in our study, this effect should be considered and further investigated in future drug delivery studies.

#### 5. Conclusion

By use of *in vivo* fluorescence imaging, we detected the accumulation of nanoparticles, nanocapsules and nanosized lipid emulsions in specific locations in the rodent ovaries. This effect was further characterised by *ex vivo* fluorescence imaging and CLSM. The investigated nanocarrier systems were completely differently composed, including multiple excipients, carrier sizes and surfaces. Based on the extensive *in vivo* and *ex vivo* studies it was found that the enrichment seems to be size dependent: whereas, polymers  $\leq 35$  nm diameter were not accumulated, all tested nanocarrier batches with diameters between 45 and 350 nm highly accumulated in the ovaries. A comparison of 3 nanoparticle batches varying in size led to the conclusion that bigger particles seemed to be more accumulated than smaller ones although this is based on a limited number of experiments. Finally it has to be noted that the accumulation of the nanocarriers in the ovaries does not necessarily need to result in a risk for the widespread use of nanoscaled carrier systems in medicine. Especially due to the fact that the accumulation is limited to special regions in the ovaries, the toxic risk for humans might be rather low. However, this effect needs to be further investigated, particularly also in other species to elucidate the mechanism of accumulation. But also the chances of these results for a new ovarian targeted therapy should be taken into consideration. Our results strongly emphasise the relevance of early explorative *in vivo* studies in the development of drug delivery systems using sensitive analytical imaging techniques, like fluorescence imaging using NIR fluorescence dyes.

#### Acknowledgements

Jürgen Vogel and Marcus Niepel are acknowledged for supporting the confocal microscopic measurements and Gerd Hause for performing the frozen section slides. We thank also Martina Henniscke and Constanze Gottschalk for the animal care. The *in vivo* studies were partly supported by the Federal State of Saxonia Anhalt (FKZ 3646A/ 0907) and the Deutsche Forschungsgemeinschaft (MA 1648/7-1). The Deutsche Forschungsgemeinschaft further supported the confocal microscopy studies (LSM: INST 271/ 250-1).

#### References

- [1] S.S. Feng, New-concept chemotherapy by nanoparticles of biodegradable polymers: where are we now? *Nanomedicine* 1 (2006) 297–309.
- [2] S.M. Moghimi, Mechanisms of splenic clearance of blood-cells and particles - towards development of new splenotropic agents, *Adv. Drug Deliv. Rev.* 17 (1995) 103–115.
- [3] I. Brigger, C. Dubernet, P. Couvreur, Nanoparticles in cancer therapy and diagnosis, *Adv. Drug Deliv. Rev.* 54 (2002) 631–651.
- [4] S.S. Suri, H. Fenniri, B. Singh, Nanotechnology based drug delivery systems, *J. Occup. Med. Toxicol.* 2 (2007) 16.
- [5] O.C. Farokhzad, R. Langer, Impact of nanotechnology on drug delivery, *ACS Nano* 3 (2009) 16–20.
- [6] V. Wagner, A. Dullaart, A.K. Bock, A. Zweck, The emerging nanomedicine landscape, *Nat. Biotechnol.* 24 (2006) 1211–1218.
- [7] H.C. Fischer, W.C.W. Chan, Nanotoxicity: the growing need for *in vivo* study, *Curr. Opin. Biotechnol.* 18 (2007) 565–571.
- [8] S.E. Dunn, A.G.A. Coombes, M.C. Garnett, S.S. Davis, M.C. Davies, L. Illum, *In vitro* cell interaction and *in vivo* biodistribution of poly(lactide-co-glycolide) nanospheres surface modified by poloxamer and poloxamine copolymers, *J. Control. Release* 44 (1997) 65–76.
- [9] R. Nakaoka, Y. Tabata, T. Yamaoka, Y. Ikada, Prolongation of the serum half-life period of superoxide dismutase by poly(ethylene glycol) modification, *J. Control. Release* 46 (1997) 253–261.
- [10] T. Yamaoka, Y. Tabata, Y. Ikada, Comparison of body distribution of poly(vinyl alcohol) with other water-soluble polymers after intravenous administration, *J. Pharm. Pharmacol.* 47 (1995) 479–486.
- [11] H.S. Choi, W. Liu, P. Misra, E. Tanaka, J.P. Zimmer, B.I. Ipe, M.G. Bawendi, J.V. Frangioni, Renal clearance of quantum dots, *Nat. Biotechnol.* 25 (2007) 1165–1170.

- [12] D.C. Litzinger, A.M.J. Buiting, N. Vanrooijen, L. Huang, Effect of liposome size on the circulation time and intraorgan distribution of amphipathic poly(ethylene glycol)-containing liposomes, *Biochim. Biophys. Acta, Biomembr.* 1190 (1994) 99–107.
- [13] D.X. Liu, A. Mori, L. Huang, Role of liposome size and res blockade in controlling biodistribution and tumor uptake of GM1-containing liposomes, *Biochim. Biophys. Acta* 1104 (1992) 95–101.
- [14] A. Schädlich, C. Rose, J. Kuntsche, H. Caysa, T. Mueller, A. Göpferich, K. Mäder, How stealthy are PEG-PLA nanoparticles? An NIR in vivo study combined with detailed size measurements, *Pharm. Res.* 28 (2011) 1995–2007.
- [15] A. Schädlich, H. Caysa, T. Mueller, C. Rose, A. Göpferich, J. Kuntsche, K. Mäder, Tumor accumulation of NIR fluorescent PEG-PLA nanoparticles: Impact of particle size and human xenograft tumor model, *ACS Nano* 5 (2011) 8710–8720.
- [16] A. Besheer, T.C. Hertel, J. Kressler, K. Mäder, M. Pietzsch, Enzymatically catalyzed HES conjugation using microbial transglutaminase: proof of feasibility, *J. Pharm. Sci.* 98 (2009) 4420–4428.
- [17] F. Leblond, S.C. Davis, P.A. Valdes, B.W. Pogue, Pre-clinical whole-body fluorescence imaging: Review of instruments, methods and applications, *J. Photochem. Photobiol. B* 98 (2010) 77–94.
- [18] I. Texier, M. Goutayer, A. Da Silva, L. Guyon, N. Djaker, V. Josserand, E. Neumann, J. Bibette, F. Vinet, Cyanine-loaded lipid nanoparticles for improved in vivo fluorescence imaging, *J. Biomed. Opt.* 14 (2009).
- [19] J. Chen, I.R. Corbin, H. Li, W.G. Cao, J.D. Glickson, G. Zheng, Ligand conjugated low-density lipoprotein nanoparticles for enhanced optical cancer imaging in vivo, *J. Am. Chem. Soc.* 129 (2007) 5798–5799.
- [20] J. Hardin, Confocal and Multi-Photon Imaging of Living Embryos, in: J.B. Pawley, B.R. Masters (Eds.), *Handbook of Biological Confocal Microscopy*, J. Biomed. Opt., 43, 2008, p. 760.
- [21] F. Rashid, R.W. Horobin, Interaction of molecular probes with living cells and tissues, *Histochem. Cell Biol.* 94 (1990) 303–308.
- [22] H.J. Lim, M.J. Parr, D. Masin, N.L. McIntosh, T.D. Madden, G.Y. Zhang, S. Johnstone, M.B. Bally, Kupffer cells do not play a role in governing the efficacy of liposomal mitoxantrone used to treat a tumor model designed to assess drug delivery to liver, *Clin. Cancer Res.* 6 (2000) 4449–4460.
- [23] S. Petersen, A. Fahr, H. Bunjes, Flow cytometry as a new approach to investigate drug transfer between lipid particles, *Mol. Pharm.* 7 (2010) 350–363.
- [24] A.C. Faure, S. Dufort, V. Josserand, P. Perriat, J.L. Coll, S. Roux, O. Tillement, Control of the in vivo biodistribution of hybrid nanoparticles with different poly (ethylene glycol) coatings, *Small* 5 (2009) 2565–2575.
- [25] M. Goutayer, S. Dufort, V. Josserand, A. Royère, E. Heinrich, F. Vinet, J. Bibette, J.L. Coll, I. Texier, Tumor targeting of functionalized lipid nanoparticles: assessment by in vivo fluorescence imaging, *Eur. J. Pharm. Biopharm.* 75 (2010) 137–147.
- [26] S.D. Tröster, U. Müller, J. Kreuter, Modification of the body distribution of poly (methyl methacrylate) nanoparticles in rats by coating with surfactants, *Int. J. Pharm.* 61 (1990) 85–100.
- [27] R. Perez-Soler, G. Lopez-Berestein, M. Jahns, K. Wright, L.P. Kasi, Distribution of radiolabeled multilamellar liposomes injected intralymphatically and subcutaneously, *Int. J. Nucl. Med. Biol.* 12 (1985) 261–263.
- [28] K.J. Harrington, G. Rowlinson-Busza, K.N. Syrigos, P.S. Uster, R.M. Abra, J.S.W. Stewart, Biodistribution and pharmacokinetics of <sup>111</sup>In-DTPA-labelled pegylated liposomes in a human tumour xenograft model: implications for novel targeting strategies, *Br. J. Cancer* 83 (2000) 232–238.
- [29] G. Thurston, J.W. McLean, M. Rizen, P. Baluk, A. Haskell, T.J. Murphy, D. Hanahan, D.M. McDonald, Cationic liposomes target angiogenic endothelial cells in tumors and chronic inflammation in mice, *J. Clin. Invest.* 101 (1998) 1401–1413.
- [30] S.D. Tröster, J. Kreuter, Influence of the surface properties of low contact angle surfactants on the body distribution of <sup>14</sup>C-poly (methyl methacrylate) nanoparticles, *J. Microencapsul.* 9 (1992) 19–28.
- [31] T.J. Daou, L. Li, P. Reiss, V. Josserand, I. Texier, Effect of poly (ethylene glycol) length on the in vivo behavior of coated quantum dots, *Langmuir* 25 (2009) 3040–3044.
- [32] L.P. Reynolds, A.T. Grazul-Bilska, D.A. Redmer, Angiogenesis in the corpus luteum, *Endocrine* 12 (2000) 1–9.